A Thesis on

PREPARATION AND CHARACTERIZATION OF $(1-x)BiFeO_3$- $xNiFe_2O_4$ (x=0, 0.3) COMPOSITE

Submitted
in partial fulfillment of the requirement for
the award of the degree of

MASTER OF SCIENCE (M.Sc.)
IN
PHYSICS

By
Keerti Chhabra
(Roll no: 301004004)

Under the supervision of
Dr. Puneet Sharma

School of Physics and Materials Science
Thapar University
Patiala (Punjab)-147004, India
July 2012

CERTIFICATE

*This is to certify that Miss KEERTI CHHABRA, Roll no. 301004004 has worked on this thesis report entitled "*PREPARATION AND CHARACTERIZATION OF (1-x) $BiFeO_3$- x$NiFe_2O_4$ (x=0, 0.3) COMPOSITE*" in partial fulfillment for award of the degree of MASTER OF SCIENCE in PHYSICS in THAPAR UNIVERSITY, PATIALA. This report is an authentic record of her own work carried out under the supervision of Dr. PUNEET SHARMA. The matter embodied in this report is one of the candidate's own record and not submitted to any other University in any part or full form for the award of such kind of degree.*

Dr. Puneet Sharma

Assistant Professor
School of Physics & Material Science

Countersigned by:

Dr. Kulveer Singh

Assoc. Prof. & Head
School of Physics & Material Science
Thapar University, Patiala

Dr. S. K. Mohapatra

Dean of academic affairs
Thapar University
Patiala.

ACNOWLEDGEMENT

Knowledge itself is a continuous process. This thesis represents not only my work at the keyboard, it is a milestone in more than one semester of work at PREPARATION AND CHARACTERIZATION OF (1-x)$BiFeO_3$ - x$NiFe_2O_4$ (x=0, 0.3) COMPOSITE. My experience has been nothing short of amazing.

Foremost, I would like to express my sincere gratitude to my esteemed and worthy supervisor **Dr. Puneet Sharma** for the continuous support for my M.Sc. thesis, for his patience, keen interest, motivation, enthusiasm, and immense knowledge. His guidance helped me in all the time of research and writing of this thesis.

I am grateful to **Dr. Kulveer Singh, Assoc. Prof. & Head** for being source of inspiration and for the infrastructural facilities which he extended to me to execute this work.

I wish to express my sincere thanks to **Dr. Manoj Sharma, P.G. Incharge, School of Material and Physics Science** for his support and encouragement.

I owe my sincere thanks to the Phd scholars-**Mr. Mintu Tyaagi**, **Miss Shiwani Sharma**, **Mrs. Samiksha Verma, Mrs. Ramneek Kaur**, **Miss Gurpreet Kaur, Miss Samita Thakur, Miss Renu Dahiya, Miss Dipti, Mr.Paramjyot Jha and Mr. Rishi Kumar** who made me believe in myself and guided me through the whole process of dissertation writing. I also extend my sincere thanks to all the staff members of School of Physics and Material Science for their support.

I thank all my friends for the stimulating discussions, for the sleepless nights we were working together before deadlines, and for all the fun we have had in the last two years.

Last but not the least, I would like to thank my family: my parents **Ved Parkash Chhabra** and **Anjani Chhabra**, for giving birth to me at the first place, taught me, loved me and supporting me spiritually throughout my life.. To them I dedicate this thesis.

Above all, hidden force by Almighty God steered me in the right direction to achieve the goal.

Keerti

KEERTI CHHABRA (301004004)

Dedicated

to

God,

My Parents

And

Teachers

ABSTRACT

In the present work bismuth ferrite powder and nickel ferrite powder were successfully made by sol-gel method using bismuth ferrite pentahydrate [$Bi(NO_3)_3.5H_2O$] and iron nitrate nonahydrate [$Fe(NO_3)_3.9H_2O$]; and nickel nitrate hexahydrate [$Ni(NO_3)_3.6H_2O$] and iron nitrate nonahydrate [$Fe(NO_3)_3.9H_2O$] respectively as raw materials. The obtained powders were characterized by XRD which showed that besides the formation of single phase $BiFeO_3$ an impurity phase was also observed. However, single phase $NiFe_2O_4$ were obtained. Composite structure of bismuth ferrite and nickel ferrite ($0.7BiFeO_3$-$0.3NiFe_2O_4$) was made and its dielectric and ferroelectric properties were compared with pure $BiFeO_3$. The dielectric properties studies showed that $0.7BiFeO_3$-$0.3NiFe_2O_4$ has smaller dielectric constant value and showed more dielectric losses as compared to pure $BiFeO_3$. The dielectric constant value at room temperature for the composite was found to be 6.02 as compared to 29.51 for pure bismuth ferrite at 10^2 Hz. The ferroelectric studies at room temperature showed a hysteresis loop for pure bismuth ferrite with remnant polarization of 5.46μC/cm^2 at coercive field of 2.48kV/cm for $BiFeO_3$ as compared to asymmetrical oval shaped hysteresis loop for $0.7BiFeO_3$-$0.3NiFe_2O_4$ composite with remnant polarisation of 0.07μC/cm^2 at coercive field of 16.96kV/cm.

Table of Contents

LIST OF FIGURE AND TABLE

FIGURE **Page No.**

CHAPTER-1

1.1 Introduction

Maxwell's equations [1] that govern the dynamics of electric fields, magnetic fields and electric charges, show that the magnetic interactions and motion of charges are intrinsically coupled to each other. These equations tell us about the unified nature of magnetism and electricity [2]. It is to be noted that there are numerous similarities (e.g. their behavior in the external fields, anomalies at a critical temperature, their domain structures) in the thermodynamics of ferroelectrics and ferromagnet; which is also expected if one looks at the equivalence of equations of electrostatics and magnetostatsics in polarizable media. These similarities are particularly striking in view of the seemingly different origins of ferroelectricity and magnetism in solids- (a) as is known, magnetism is related to ordering of spins of electrons in incomplete ionic shells (b) whereas, ferroelectricity results from relative shifts of negative and positive ions that induce surface charges. There are, however cases where these degrees of freedom couple strongly. For example, for spintronic materials at large fields, the effects of spins on the transport properties of solids (and vice versa) allow the possibility to control one by other.

The suggestion of strong coupling of magnetic and electric degrees of freedom in insulators can be traced back to Pierre Curie [3], but real beginning of this field started in 1959 with a short remark by Landau and Lifshitz [4] in a volume of course of theoretical physics that are described in the following subsection 1.1. The quest for these materials are propelled by the prospect of controlling charges by applied magnetic field and spins by applied voltages, to construct new forms of multifunctional devices.

1.2 Multiferroics

1.2.1 Definition

As the name suggests **multiferroic** are materials those posses more than one of the so called ferroic (ferroeletricity / ferromagnetism / ferroeleasticity) properties. In recent years this term is loosely used for the materials in which magnetism and ferroelectricity coexist. In 1894, P.Cuire [3] predicted that crystals could be simultaneously ferromagnetic and ferroelectric and magnetization in the crystal can be induced by the application of electric

field and vice versa. This effect is known as "**magneto electric effect**" and the coupling between ferroelectric and magnetic interactions is known as "**magneto electric coupling**". It is clear from the definition of magneto electric coupling that the coexistence of ferroelectric and ferromagnetic orders is a necessary condition for the material to be classified as a magneto electric material; however, magneto electric coupling is an independent phenomenon that need not arise in all materials that are both magnetically and electrically polarizable. In practice, it is likely to arise in all materials that are both magnetically and electrically polarizable, either directly or via strain. This concept is pictorially depicted by several authors [5,6] through a schematic diagram as shown in Fig.1.1. In this diagram, ferromagnets (ferroelectrics) form a subset of magnetically (electrically) polarizable materials such as paramagnets and antiferromagnets (paraelectrics and antiferroelectrics) shown. The intersection of ferroelectric and ferromagnetic materials represents materials that are multiferroic and the smallest circle in the middle represents the materials that would show magneto electric coupling.

The materials which have coexistence of ferroelectric and magnetic orders and exhibit magneto electric coupling are called "**Magneto electric Multiferroics**".

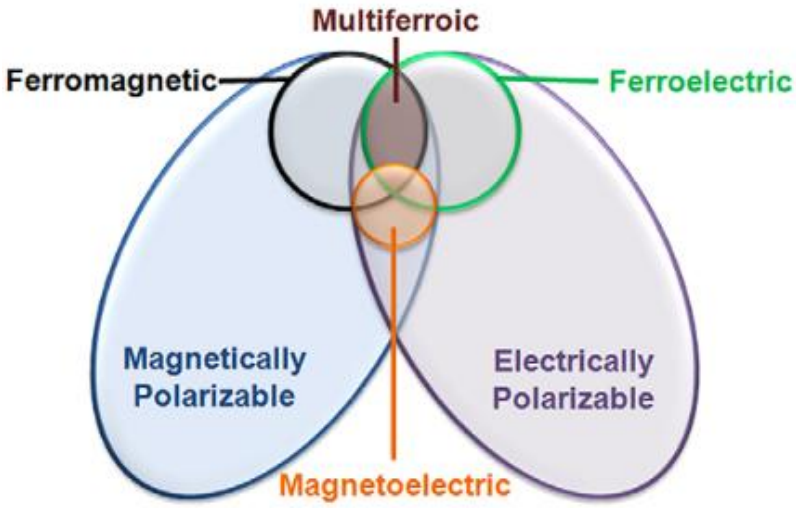

Fig.1.1 Relationship between multiferroic and magnetoelectric materials [6].

1.2.2 Requirements for Magnetoelectric Multiferroics

Although the experimental evidences of multiferroics and magnetoelectric phenomenon were started in the first half of 20^{th} century, the numbers of the materials that exhibit magnetoelectric coupling were found to be rare. The coexistence of ferroelectric and magnetic orders itself is a challenging problem. In 2000, Hill discussed [7] in her review, the conditions required for ferroelectricity and ferromagnetism to be compatible in oxides; however, she also declared that these conditions are contradictory to each other and area difficult to be met in a material. The limiting factors which restrict the simultaneous existence of ferroelectricity and ferromagnetism are as given below.

1.2.2.1 Symmetry

The magnetoelectric effect was predicted by P.Curie [3] on the basis of symmetry considerations. The primary conditions for ferroelectricity are the non-centrosymmetric structure, which allows the dipole formation and spontaneous polarization. There are 31 (out of 122) Shubnikov Heesch point groups that allow spontaneous electric polarization and 31 that allow spontaneous magnetization [8]. There is only 13 Shubnikov points, which allow both spontaneous magnetization and spontaneous electric polarization in same phase. The symmetry considerations itself restrict the number of multiferroics.

1.2.2.2 Electrons occupancy in d-orbital

In most of the perovskite multiferroics (ABO_3) the B-site is occupied by transition metals. According to electronic configuration, transition elements have empty, fully filled or partially filled d-orbitals that contribute to the electrical, magnetic and other physical properties of the material.

1.2.3 Types of Multiferroics

The microscopic origin of magnetism is basically the same in all magnets; it is the presence of localized electrons, mostly in the partially filled *d* or *f* shells of transition metal or rare earth ions, which have corresponding localized spin, or magnetic moment. Exchange interactions between localized moments lead to magnetic order. However the situation is different in case of ferroelectrics. There are several different microscopic origins of ferroelectricity and accordingly one can have different types of Multiferroics.

Generally the Multiferroics are categorized in two groups: (i) type I Multiferroics and (ii) type II Multiferroics, on the basis of the origin of ferroelectricity in them [9].

1.2.3.1 Type I Multiferroics

This group of Multiferroics contains those perovskites in which ferroelectricity and ferromagnetism have different sources (cations at A-site and B-site respectively). These materials show weak magnetoelectric coupling. In these materials, ferroelectricity typically appears at higher temperatures than magnetism and they exhibit large spontaneous polarization. Examples are $BiFeO_3$ (T_c ~ 1110 K, T_N ~ 643 K, P ~ 90 μC/cm^2), $YMnO_3$ (T_c^{FE} ~ 914 K, T_N ~ 76 K, P ~ 6 μC/cm^2). These materials have been extensively studied since 1960's. However, major challenge in these materials is to enhance the values of magnetoelectric coupling coefficient. Type I Multiferroics are further classified in many subclasses on the basis of origin of ferroelectricity.

(i)*Ferroelectricity due to shifting of B-cation*

In the literature, there are a number of perovskites materials reported that show ferroelectricity due to non-centrosymmetry of B- site cation [10]. However, as discussed above the B-site cation in perovskites usually is the cause of magnetic ordering (if any) in these perovskites [11]. Clearly, "d^0 vs. d^n problem" as discussed in the above section creates difficulty in such situations.

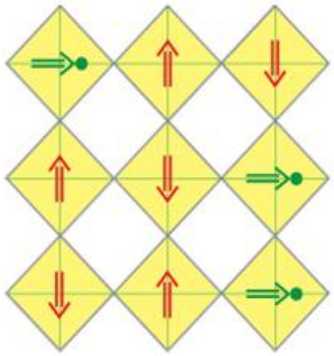

Fig.1.2. In "*mixed*" perovskites with ferroelectricity active d^0 ions (green circles) and magnetic d^n ions (red circles), shifts of d^0 ions from oxygen octahedral (yellow plaquettes) lead to polarization (green arrows), coexisting with magnetic order (red arrows) [9].

(ii) *Ferroelectricity due to lone pairs*

These multiferroic materials exhibit ferroelectricity due to lone pair at A-site cation. Most of Bismuth (Bi) and Lead (Pb) based perovskites show ferroelectricity *due to lone pair*, for example $BiFeO_3$, $BiMnO_3$, and $PbVO_3$. In these materials Bi^{3+} and Pb^{2+} have two outer 6*s* electrons that do not participate in chemical bonds. These electrons are called "*lone pairs*" or sometimes dangling bonds. Microscopically, one can explain the origin of ferroelectricity in these compounds by the ordering of these lone pairs (with certain admixture of *p*-orbitals) in the direction of electric field. The magnetism in these materials is originated from B-cation.

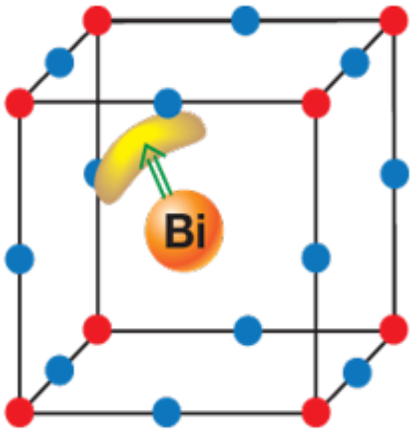

Fig.1.3. In materials like $BiFeO_3$ and $PbVO_3$, the ordering of lone pairs (yellow "lobes") of Bi^{3+} and Pb^{2+} ions (orange), contributes to the polarization (green arrow) [9].

(iii) *Ferroelectricity due to charge ordering*

This is another group of ferroelectrics, in which the electric polarization is induced *due to the non-centrosymmetry of charges*. The non-centrosymmetry of charges is normally observed in transition metal compounds (especially transition metal ions with different metal states) e.g. $Pr_{0.5}Ca_{0.5}MnO_3$ or in Nickelates $RNiO_3$ [12, 13].

(iv) *"Geometric" ferroelectricity*

In this category of Multiferroics, some geometric disorder in the lattice causes ferroelectricity. For example in case of $YMnO_3$, ferroelectricity has nothing to do with individual cations, but is caused by the tilting of practically rigid MnO_5 block with respect to Y-ions [14]. This tilting occurs just to provide closer packing, and as a result the oxygen ions moves closer to the rather small Y ions.

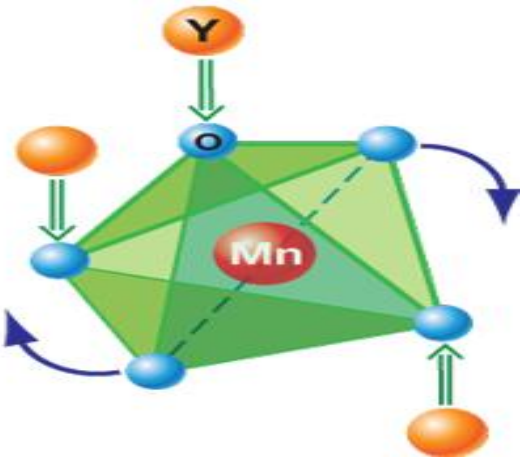

Fig.1.4 The "geometric" mechanism of generation of polarization in $YMnO_3$ [14] describes the tilting of a rigid MnO_5 block with a magnetic Mn remaining at the center. Because of the tilting, the Y-O bonds form dipoles (green arrows), and there appears two"up" dipoles per one "down" dipole so that the system becomes ferroelectric (and multiferroic when Mn spins order at lower temperatures) [9].

1.2.3.2 Type II Multiferroics (Magnetic Multiferroics)

The materials in which the ferroelectricity is originated from magnetism and implies strong magnetoelectric coupling. However the polarization in these materials is usually much smaller (10^{-2} $\mu C/cm^2$). These Multiferroics are recently discovered. $TbMnO_3$ and $TbMn_2O_5$ are typical examples of these materials [15, 16]. Kimura *et al* [15] demonstrate strong influence of magnetic field on electric polarization. In $TbMnO_3$, the polarization rotates (or "flops") by 90 degrees when a critical field is applied in a certain direction [15]. Influence of magnetic field is even stronger in case of $TbMn_2O_5$ [16]. The polarization changes sign with magnetic field. Since the discovery of these materials, a number of other type-II Multiferroics with strong magnetoelectric coupling have been discovered and studied. On the basis of mechanism of multiferroic behavior, one can divide type-II Multiferroics in two categories.

(i)*Spiral Type-II Multiferroics*

In this type of Multiferroics, the ferroelectricity appears in conjunction with a spiraling magnetic phase, mostly cycloid type. $TbMnO_3$, $Ni_3V_2O_6$ and $MnWO_4$ are typical examples of this type of multiferroics. Therefore, these type-II multiferroics are usually found in frustrated magnetic systems.

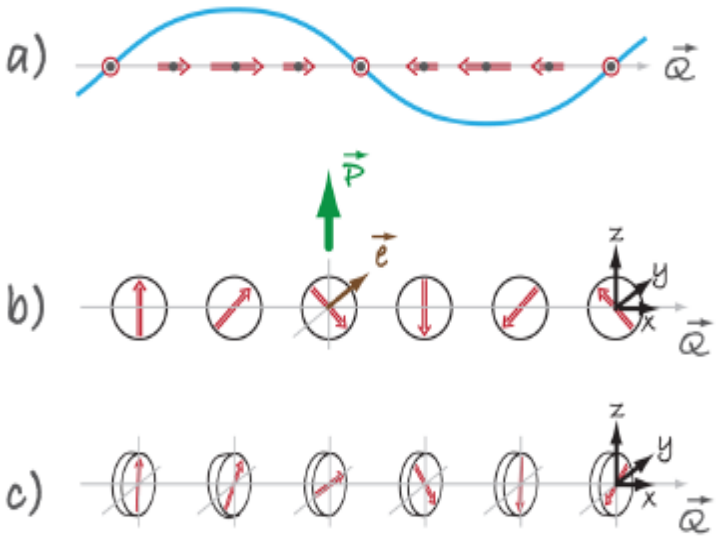

Fig.1.5 Different types of spin structures relevant for type-II Multiferroics (a) Sinusoidal spin density wave, in which spins point along one direction but vary in magnitude. This structure is centrosymmetic and consequently not ferroelectric. (b) The cycloidal spiral with the wave vector **Q** = Qx and spins rotating in the (x,z)-plane. It is in this case where one finds nonzero polarization, Pz ≠ 0. (c) In a so-called "proper screw" the spins rotate in a plane perpendicular to **Q**. Here the inversion symmetry is broken, but most often it does not produce polarization, although in certain cases it might [17].

(ii) *Type-II Multiferroics with Collinear Magnetic Structures*

In this group of Type-II multiferroics ferroelectricity appears in collinear magnetic structures; *i.e.*, all magnetic moments are aligned along a particular axis without the necessary involvement of spin-orbit interaction. Polarization can appear in these materials as a consequence of exchange striction because the magnetic coupling varies with atomic positions. The simplest example of this type of multiferroics is Ca_3CoMnO_6 [18].

1.2.4 Applications of multiferroics

Most of the research in multiferroics has been curiosity driven basic research, but there are a number of ideas for device applications based on multiferroic materials. One of the more popular ideas is that multiferroic bits may be used to store information in the magnetization *M* and the polarization *P*. The feasibility of such a 4 stage memory (two magnetic M↑↓ and two ferroelectric P↑↓) has been demonstrated recently [19, 20, 21]. Such a memory does not require the coupling between ferroelectricity and magnetism; a cross

coupling would be even disastrous. If magneto-electric coupling is present, device applications could be realized where information is written magnetically, but stored in the electric polarization, leading to non-volatile memory. Multiferroics bits could also be used to increase the magnetic anisotropy to increase the decay time for magnetic storage. Other applications include magnetically field-tuned capacitors with which the frequency dependence of electronic circuits could be tuned with magnetic fields, or multiferroic sensors which measure magnetic fields through zero-field current measurements.

1.3 Status of Multiferroicity in Bi-Based Compounds

Bi-based compounds are of main interest due to their multiferroic behavior. There are many Bi- based perovskite compounds in which B-site is accommodated by transition metals e.g. $BiFeO_3$ [22], $BiMnO_3$ [23], $BiCrO_3$ [24] etc. However $BiFeO_3$ (BFO) and $BiMnO_3$ (BMO) [23, 24, 25] are most extensively studied compounds due to the evidence of coexistence of ferroelectricity and magnetic ordering in them. These compounds fall into the category of "**type-I multiferroics**". Ferroelectricity originates from the alignment of lone pair of Bi^{3+} ion and magnetism comes from B-site atom (Mn or Fe).

1.3.1 Bismuth Ferrite (BFO)

$BiFeO_3$ is one of the most extensively studied multiferroic material in recent years [17, 22, 24] and it is the only material known to exhibit magnetic order (T_N= 643 K) and ferroelectric order (ferroelectric transition temperature T_c^{FE}= 1103 K) at room temperature. The properties of the material are discussed in this section.

1.3.1.1 Synthesis and Phase Diagram of $BiFeO_3$

BFO is usually prepared from equal parts of Bi_2O_3 and Fe_2O_3. But BFO is very prone to show parasitic phases that tend to nucleate at grain boundaries and impurities. There were reports in literature in which the difficulties of single phase formation of BFO were discussed. So it is a challenge to prepare single phase $BiFeO_3$. The phase diagram of Bi_2O_3 and Fe_2O_3 is shown in the Fig.1.6. It is clear from the phase diagram that the stochiometry is an important parameter to get a single phase for BFO. It is also noted that the calcination temperature and melting point of BFO is very close to each other due to which the BFO can decompose to these starting materials as shown in equation.

$$2\ BiFeO_3 \longrightarrow Fe_2O_3 + Bi_2O_3$$

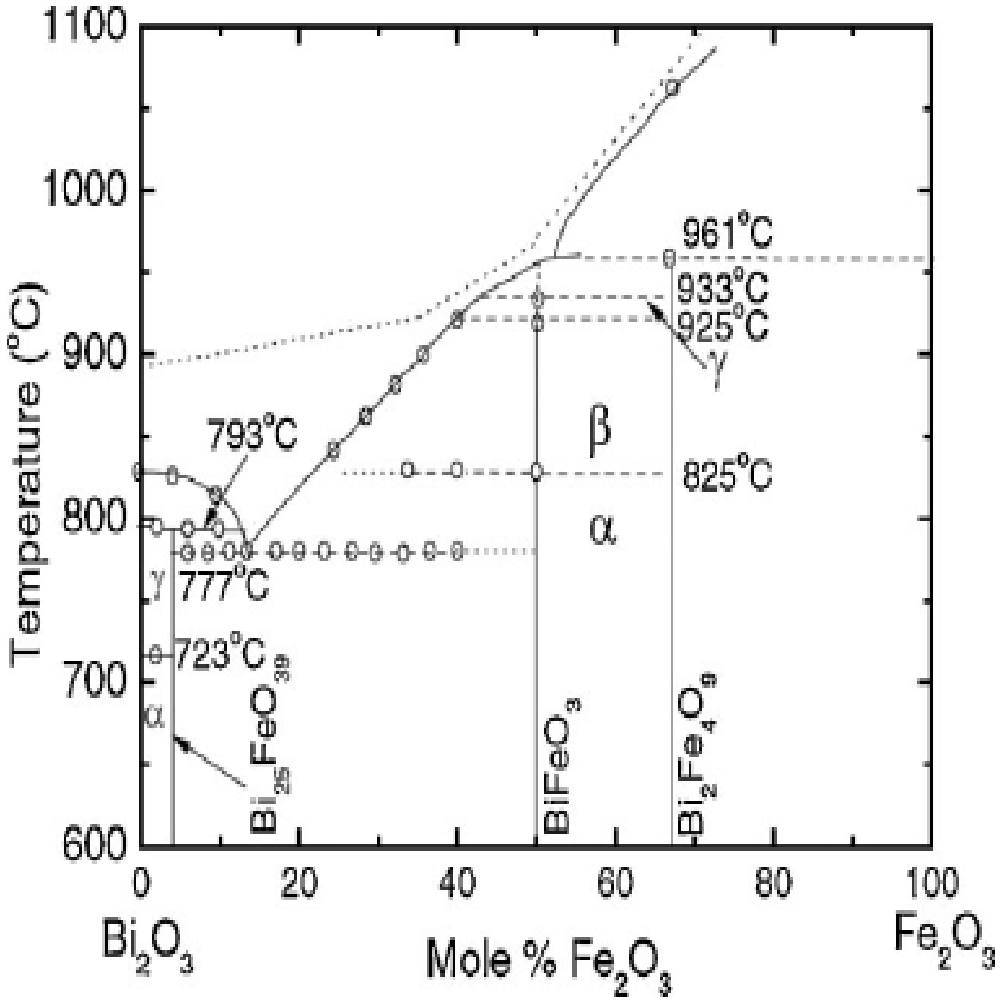

Fig.1.6 Phase Diagram of Bi_2O_3 –Fe_2O_3 system.

1.3.1.2 Crystal structure

BFO exhibits rhombohedrally distorted structure with space group symmetry R3c at room temperature as in fig. 1.7. The corner positions are occupied by Bi ions, at the center of the cube lies the transition Fe ion and the face centers are occupied by the oxygen ions. The lattice parameters of the rhombohedral unit cell are a = 5.59 Å and α = 60.68°. In such a distorted structure, the R3c symmetry permits the development of spontaneous polarization (Ps). The Fe-O-Fe angle controls the magnetic exchange and orbital overlap between Fe and O, and as such it determines the magnetic ordering temperature and the conductivity.

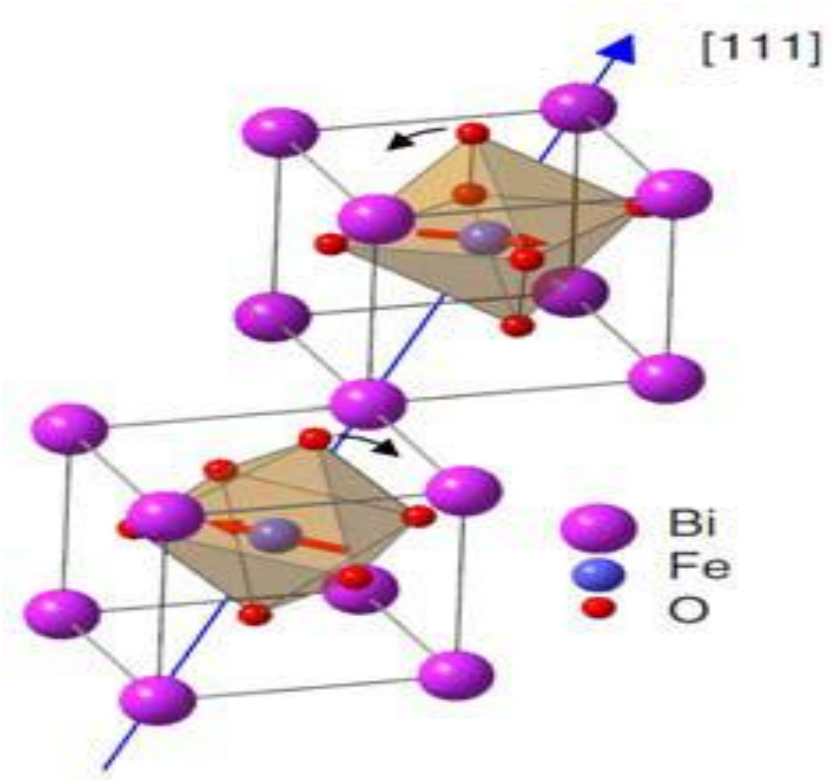

Fig. 1.7 Crystal structure of $BiFeO_3$

Each Fe^{3+} spin is surrounded by six antiparallel spins on the nearest Fe neighbours, that is, a G-type antiferromagnet. This means that the Fe magnetic moments are coupled ferromagnetically within the pseudocubic (111) planes and antiferromagnetically between adjacent planes.

1.3.2 Limitations of $BiFeO_3$

Although BFO is a unique material with the coexistence of ferroelectricity and anti ferromagnetism but there are some difficulties due which this material in not very useful for technical application.

- **Difficulty in Formation of single phase in BFO:** To get better magnetoelectric coupling as well as multiferroic properties the pure $BiFeO_3$ is required. But it is already discussed that it is a challenging problem to get pure BFO. There are methods suggested by authors to get rid of this problem.

- **Electrical Resistivity:** As discussed in the above section that BFO exhibits semiconducting behavior at and above room temperature, which does not allow

electric poling and causes high dielectric losses in the sample at room temperature. Due to this, it is difficult to measure the ferroelectric properties of BFO at and above room temperatures.

- **Weak Magnetoelectric Coupling:** Theoretical calculations predict that a large difference between the transition temperatures T_c and T_N causes weak ME coupling in BFO. If the ME coupling is weak, corresponding ME voltage signal would also be weak. So it is difficult to measure ME coupling of the material.

- **Cyclodial Spin Structure:** The existence of cyclodial spin structure in BFO averages out any linear magnetoelectric coupling between polarization and magnetization. So it is very difficult to measure the linear magnetoelectric coupling at lower magnetic fields. However, higher order ME coupling can be measured. The anti ferromagnetic vector is averaged out to zero over one cycloidal period leads to zero remnant magnetization and induced magnetization is proportional to magnetic field.

1.4 Nickel Ferrite

Spinel ferrites [26] have been studied for many years both regarding their magnetic behaviour and correlated nature in conjunction with their structural properties. Spinel is a type of mineral ($MgAl_2O_4$) whose chemical composition is found in the ratio of one ion with a positive two charge, two different ions with a positive three charge and four oxygen atoms with a negative two charge. Spin dependent gap should result in spin-dependent barrier for tunneling of electrons through the insulator, giving rise to spin filtering. Since the tunneling probability depends exponentially on the barrier height, the spin filtering efficiency can be very high. Candidates for spin filters include such spinel ferrites as $NiFe_2O_4$, $CoFe_2O_4$ and $MnFe_2O_4$ [27]. Recently, $NiFe_2O_4$ barrier showed filtering efficiency of upto 22%. Nanosize spinel ferrite particles have attracted considerable attention and continued efforts to investigate them for their technological importance to the microwave industries, high speed digital tap or disk recording, repulsive suspension for use in levitated railway systems, ferrofluids, catalysis and magnetic refrigeration systems [28-30].

These spinel ferrites belong to the same family as magnetite (Fe_3O_4) which has been most thoroughly studied. The spinel ferrites of interest to the present study have a general chemical formula of the form AB_2O_4 and crystallize in the face-centred cubic structure. In spinels the

oxygen ions are forming a cubic close packed structure. Concerning the distribution of the cations we have to distinguish between two kinds of spinels:

1.) The first one is the so called "normal spinel", which has the general formula AB_2X_4. In this structure the A-cations are occupying 1/8 of the tetrahedral holes and the B-cations are occupying ½ of the octahedral holes. Example $ZnFe_2O_4$.

2.) The second type of spinels is the so called "inverse spinel". It has the general formula $B[AB]O_4$. In this structure the B-cations are occupying 1/8 of the tetrahedral holes and the second B- and the A-cations are occupying ½ of the octahedral holes. An example for an inverse spinel is Fe_3O_4 [31, 32].

$NiFe_2O_4$ is a ferromagnetic insulator and this compound has the Curie temperature of 850 K. The ground state of nickel ferrite is found to be insulating and of the inverse spinel kind. Ferrimagnetic property of the material arises from magnetic moments of anti-parallel spins between Fe^{3+} ions at tetrahedral sites and Ni^{2+} and Fe^{3+} ions at octahedral sites [33]. It has high Neel temperature, low microwave loss, and low magnetostriction. Nickel ferrite is a soft high frequency magnetic material having high electrical resistivity.

1.4.1 Structure of Nickel Ferrite

Nickel ferrite is an ideal example of inverse spinel ferrite. In nickel ferrite, A sites are occupied by ferric ions (Fe^{3+}), and B sites are occupied by the 1:1 mixture of nickel ions (Ni^{2+}) and Fe^{3+} ions. Ni^{2+} ions are located on B sites and octahedrally coordinated by surrounding O^{2-} ions. Thus compound can be represented by the formula $(Fe^{3+})_A[Ni^{2+}Fe^{3+}]_BO_4^{2-}$.

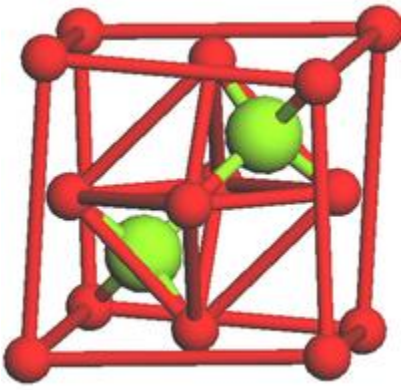

Fig. 1.8 Inverse spinel structure

The local symmetry of octahedral results in the singlet ground state of Ni^{2+} ($3d^8$), and consequently, vanishing of the expectation value of the orbital angular momentum. This effect is called 'quenching' of orbital angular momentum.

1.4.2 Uses

- This material is largely used in electric and electronic devices and in catalysis [34].
- Nickel ferrite is a suitable material for microwave applications. It is an excellent core material for power transformers in electronics and telecommunication applications [35].
- Nickel ferrite and its derivatives have been tried as inert anodes for electrometallurgical applications particularly for the production of aluminium using Hall Heroult process [36].
- It is a major constituent of the corrosion oxides that form on nickel base Fe-Ni-Cr alloys exposed to reactor coolant in many nuclear power reactors [37].

CHAPTER-2
LITERATURE REVIEW

In the present chapter, research work carried out on bismuth ferrite and nickel ferrite prepared by wet chemical methods has been summarized. Further the important work carried out on magnetoelectric composites in the thin film as well in bulk form has been discussed.
The literature for Bismuth ferrite:

Kim *et al* (2005) [38] synthesized high purity BFO R-phase powders with particle size of ~200 nm by the sol–gel process followed by leaching in diluted nitric acid. The dielectric constant of the BFO R-phase was found to be ~15 in the frequency range of 10^4 ~ 10^6 Hz at room temperature.

Chen *et al* (2006) [39] synthesized insulating and single-phase $BiFeO_3$ ceramics by rapid sintering at 800^{o}C using sol gel derived fine powders. The grains of 2–6 μm in diameter heap densely up in the ceramics. The leakage current density of the ceramics remains lower than $3.02x10^{-4}$A/cm^2 under the poling field below 119kV/cm. The main conduction mechanism is space-charge-limited current generated from oxygen vacancies. The ceramics exhibit a saturated ferroelectric hysteresis loop with a large remnant polarization $2P_r$ of 56μC/cm^2 at room temperature**.**

Pandu *et al* (2010) [40] concluded that it is possible to synthesize $BiFeO_3$ at low temperature using sol-gel technique. From XRD pattern it is seen that crystallite size increases as sintering temperature increases. As the crystallite size increases with increasing temperature the lattice parameter decreases. The Curie temperature of pure $BiFeO_3$ is 814^{o}C which is very close to the ideal value 827^{o}C found by dielectric measurement.

Kosec *et al* (2010) [41] characterized the ferroelectricity of $BiFeO_3$ ceramics by strong domain-wall pinning most likely caused by charged defects. The domain-wall mobility can be increased considerably by preventing the diffusion of these defects into their stable configuration, from which they stabilize the domain walls. The quenched ceramics exhibited a higher remnant polarization and permittivity, both originating from the increased domain-wall mobility.

Chen *et al* (2011) [42] synthesized pure perovskite bismuth ferrite ($BiFeO_3$) microspheres and microrectangulars by using the sol–gel–hydrothermal method at 180°C for 12 h, using initial KOH concentrations of 6 M and 10 M respectively. Increasing both reaction temperature and time had a positive effect on the formation of $BiFeO_3$ crystallites.

Bhole *et al* (2011) [43] synthesized $BiFeO_3$ ceramics by solid state and showed that it has the rhombhohedral perovskite structure. The ferroelectric measurement reveals the ferroelectric nature of $BiFeO_3$ with saturation and remnant polarizations of Ps = 0.26μC/cm^2, Pr = 0.11μC/cm^2 respectively. The dielectric constant and loss as a function of temperature shows the dielectric constant and loss increases with increasing temperature.

The literature for nickel ferrite:

Albuquerque *et al* (2001) [44] synthesized ultrafine powders of Ni-ferrite with particle diameter ranging from 4 to 15 nm by co-precipitation followed by annealing at temperatures between 300^{o}C and 600^{o}C. It is also observed that Ni-ferrite nanoparticles exhibit superparamagnetic relaxation and coercivity as high as 168Oe, that is nearly two times the coercivity of bulk Ni-ferrite.

Azadmanjiri *et al* (2006) [45] synthesized nickel ferrite by sol-gel and studied the effect of pH value and amount of citric acid on characteristics of nickel ferrite powder. It is found that ferrite powder could be formed at all pH values but pH 7 is the most suitable value. The particle size of the powder synthesized depends on the ratio of metal nitrates to citric acid.

Jacob *et al* (2011) [46] synthesized nickel ferrite by sol-gel method and found that as the annealing temperature is increased, particle size and saturation magnetization also increases. Sol–gel derived particles annealed at 600°C exhibits hematite (Fe_2O_3) phase also.

Sivakumar *et al* (2011) [47] synthesized nickel ferrite nanoparticles through sol-gel auto-combustion method which is a unique combination of the ignition and the chemical gelatine processes and has the advantages of simple preparation, cost-effective and gentle chemistry route resulting in ultra fine and homogeneous powder. The ability to obtain single

phase nickel ferrite magnetic nanoparticles with controllable particle size and size distribution improves its adequacy in a wide range of technological applications.

The literature for the composites:
We have studied the preparation methods and properties of bulk and thin films of $BiFeO_3$-AB_2O_4 composites.

Zheng *et al* (2006) [49] discovered that self-assembled perovskite-spinel nanostructures can be controlled simply by selecting single-crystal substrates with different orientations. In a model $BiFeO_3$-$CoFe_2O_4$ system, a (001) substrate results in rectangular-shaped $CoFe_2O_4$ nanopillars in a $BiFeO_3$ matrix; in contrast, a (111) substrate leads to triangular-shaped $BiFeO_3$ nanopillars in a $CoFe_2O_4$ matrix, irrespective of the volume fraction of the two phases. This dramatic reversal is attributed to the surface energy anisotropy as an intrinsic property of a crystal.

Q.Zahan *et al* (2006) [50] investigated the structure and the interface chemistry of epitaxial $BiFeO_3$–$NiFe_2O_4$ nano composite thin films on $SrTiO_3$ (001) substrates using the *Z*-contrast imaging and the electron exit-wave reconstruction methods at the atomic scale. The results show that the $NiFe_2O_4$ pillars are non wetting with respect to the substrate and exhibit (111) facets at the surface. The interface between $BiFeO_3$ and $NiFe_2O_4$ lies in the (110) planes and is semi coherent. The atomic configuration of the interface, with the $BiFeO_3$ layer bonding to the $[Ni,Fe]O_2$ layer, was shown to have the maximized structure continuity and minimized interface charging.

Crane *et al* (2009) [52] studied multifunctional thin film nanostructures containing soft magnetic materials such as nickel ferrite. The nanostructures composed of ferrimagnetic $NiFe_2O_4$ pillars in a multiferroic $BiFeO_3$ matrix can be tuned magnetically by altering the aspect ratio of the pillars by depositing films of varying thickness. Magnetic anisotropy is studied using ferromagnetic resonance, which shows that the uniaxial magnetic anisotropy in the growth direction changes sign up on increasing the film thickness. The magnitude of this anisotropy contribution can be explained via a combination of shape and magnetostatic effects, using the object-oriented micromagnetic framework (OOMMF).

Yan *et al* (2009) [53] reported the direct measurement of a magnetoelectric (ME) exchange between magnetostrictive $CoFe_2O_4$ nanopillars in a piezoelectric $BiFeO_3$ matrix for single layer nano composite epitaxial thin films grown on (001) $SrTiO_3$ substrates with $SrRuO_3$ bottom electrodes. The ME coefficient was measured by a magnetic cantilever method and had a maximum value of ~20mV/cm Oe. The films possessed saturation polarization ($60\mu C/cm^2$) and magnetization (410emu/cc) properties equivalent to bulk values, with typical hysteresis loops.

Babu *et al* (2010) [54] synthesized multiferroic composites of $NiFe_2O_4$ (NFO) and $BiFe_{0.5}Cr_{0.5}O_3$ (BFCO) by sol-gel method. NFO-BFCO forms a two-phase composite. The composite has a larger magnetization and dielectric constant than those of both parent compounds, due to the effects of interfacial strain on BFCO. Furthermore, the ME response in NFO-BFCO is about one time larger than that of BFCO, revealing the success of magnetic control of the dielectric response via the mechanical coupling, which can be exploited in the future applications of multiferroic composites.

Uniyal *et al* (2010) [55] prepared nano composites of $xZnFe_2O_4–(1−x)BiFeO_3$, x = 0.1, 0.2, 0.3, 0.4 by sol–gel technique. The samples have been calcined at various temperatures ranging from 500 to 800^oC and then the effect of annealing temperature on dielectric and magnetic properties is studied. Transmission electron microscopy revealed the formation of powders of nano order size and the crystal size was found to be around 30 nm. The magnetic behaviour is found to be strongly dependent upon concentration of Zn ferrite phase and annealing temperature. Enhancement of dielectric constant is observed for the samples with high ferrite concentration and antiferromagnetic Néel temperature is also evident for the samples with maximum ferrite concentration.

Kumar *et al* (2010) [56] prepared spinel-perovskite nano composites of $xCrFe_2O_4–(1-x)\ BiFeO_3$ with x= 0.0, 0.1, 0.2, 0.3, 0.4 by sol gel method. The XRD showed the phase formation of nano composites at 700^oC. Particle size was observed to be ~100 nm by TEM. The variation of dielectric constant and dielectric loss with frequency showed dispersion in the low frequency range. Magnetization was found to increase with increasing concentration of ferrite content. Dielectric analysis showed the conducting behavior at higher temperature. Magneto-capacitance was also observed in the prepared nano composites which may be the sign of magneto electric coupling in the synthesized nano composites at room temperature.

CHAPTER-3
EXPERIMENTAL PROCEDURE

3.1 Sol-gel method

The sol-gel process is a wet-chemical technique widely used in the fields of materials science and ceramic engineering. Such methods are used primarily for the preparation of materials (typically metal oxides) starting from a colloidal solution (*sol*) that acts as the precursor for an integrated network (or *gel*) of either discrete particles or network polymers. Typical precursors are metal alkoxides and metal salts (such as chlorides, nitrates and acetates), which undergo various forms of hydrolysis and polycondensation reactions.

3.2 Preparation of Bismuth Ferrite

Bismuth ferrite powder was prepared by Sol-gel method followed by annealing. The raw materials used for the experiment were bismuth nitrate pentahydrate [$Bi(NO_3)_3.5H_2O$] with 98% purity, iron nitrate nonahydrate [$Fe(NO_3)_3.9H_2O$] with 98% purity, 2-methoxyethanol and acetic acid. The procedure for the preparation is as follows:

The molar ratio of Bi to Fe was 1:1. Firstly, bismuth nitrate pentahydrate (5 mol% excess) was dissolved at room temperature in the 2-methoxyethanol and acetic acid mixture for about an hour. When the solution becomes transparent, it was mixed with iron nitrate nonahydrate by constant stirring at room temperature for another one hour. The resultant solution was transparent, blackish red and clear. The solution was then heated at 50-60^oC with constant stirring for four hours. Then the temperature was slowly increased to 80^oC, till there was an immense evolution of brown fumes, towards the end of the reaction a fluffy brown mass (gel) was obtained at the base of beaker which get converted into powder. The so obtained powder was then annealed at 800^oC with holding time of one hour in a tubular furnace with heating and cooling rate maintained at 5^oC per minute. Phase identification of the annealed powder was carried out by X-ray diffraction instrument X'Pert ProPanlytical. Further the powder was pressed into pellets (using polyvinyl alcohol as binder) of 10mm diameter die under 10 ton/cm^2 pressure using hydraulic press. The pressed pellets were sintered at 850^oC for one hour. For dielectric measurements, the sintered pellets were coated on both sides by Ag paste. The dielectric measurements were carried out by LCR meter Agilent 4284A (frequency range 20 Hz to 1MHz) and *P-E* loop of the pellet were carried out by the scan Agilent 4284A

(frequency range 20 Hz to 1MHz). Fig. 3.1 shows the flow diagram of the preparation of BFO powder.

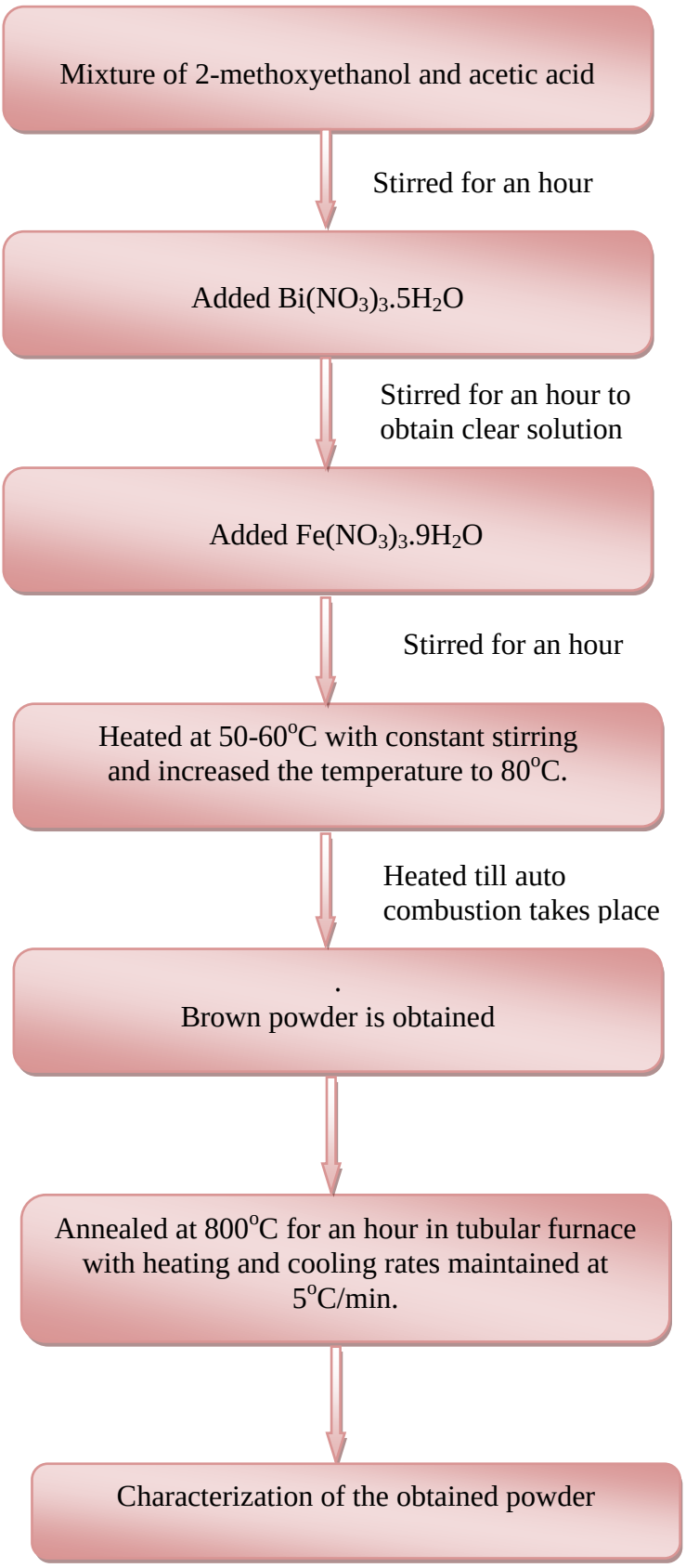

Fig. 3.1 Flow chart for BFO powder preparation

3.3 Preparation of Nickel ferrite powder

Nickel ferrite powder was also prepared by sol-gel method followed by annealing. The raw materials used for the experiment were nickel nitrate hexahydrate [$Ni(NO_3)_3.6H_2O$] with 98% purity, iron nitrate nonahydrate [$Fe(NO_3)_3.9H_2O$] with 98% purity and citric acid. The preparation process is described as follows:

The molar ratio of Ni to Fe was 1:2. First, a certain amount of citric acid was weighed and dissolved in diluted water; then $Ni(NO_3)_2 \cdot 6H_2O$ and $Fe(NO_3)_3 \cdot 9H_2O$ were dissolved in it with a molar ratio of total nitrates to citric acid of 1:1. A small amount of ammonia was added into the solution to adjust the pH value to about 7 and stabilize the nitrate–citrate solution. During this procedure, the solution was continuously stirred using a magnetic agitator and kept at a temperature of 50°C. Then, the mixed solution was poured into a dish, heated slowly to 100°C and stirred constantly until the viscosity and color changed as the solution turned into a porous dry gel, the dried gel simultaneously burnt in a self-propagating combustion manner until all the gel was completely burnt out to form a loose powder. The as synthesized powder was then annealed at 1100^oC with holding time of four hours in a tubular furnace with heating and cooling rate maintained at 5^oC per minute. Phase identification of the annealed powder was carried out by X-ray diffraction instrument X'Pert ProPanlytical. Fig. 3.2 shows the flow chart for the $NiFe_2O_4$ powder preparation:

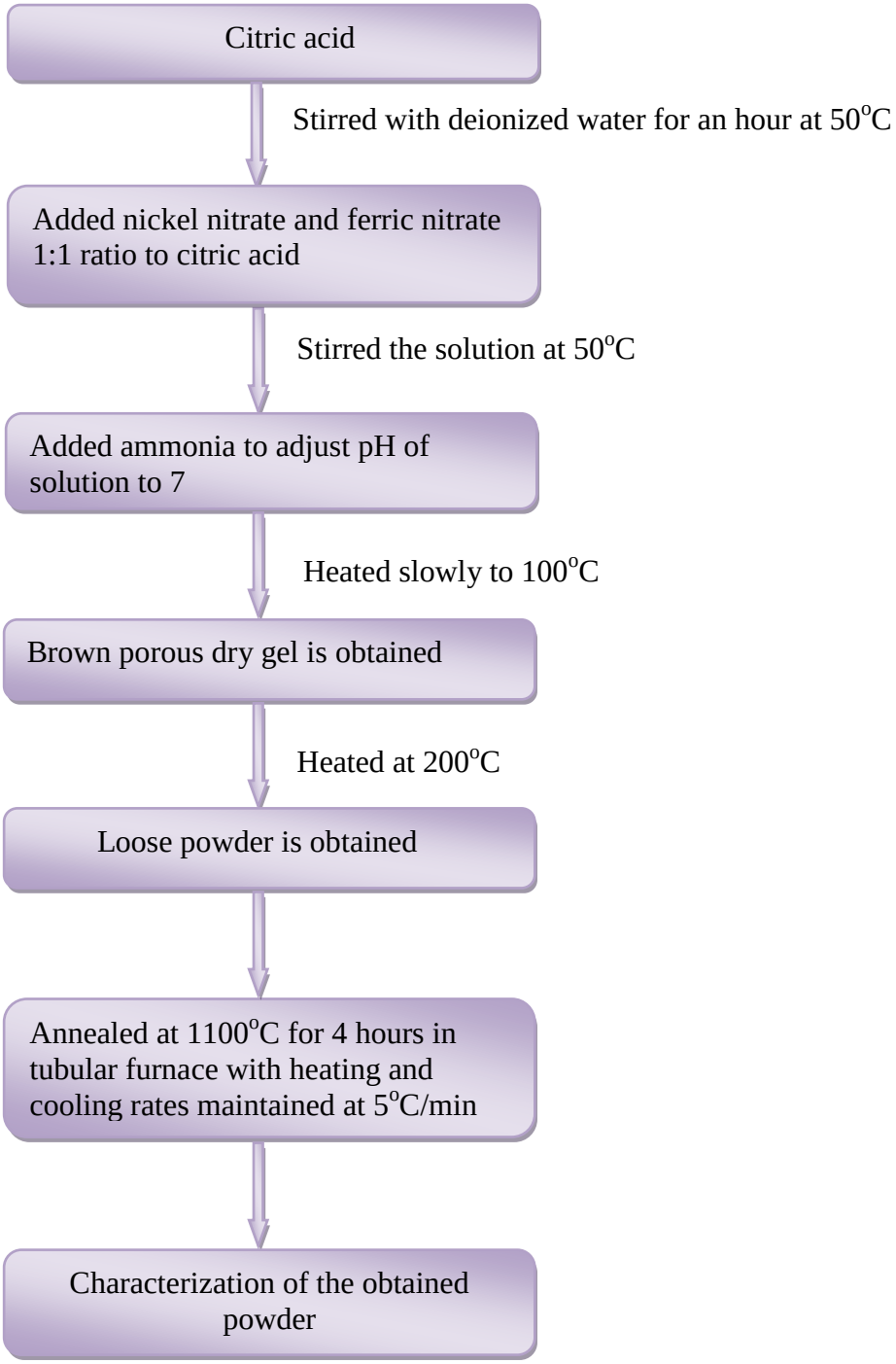

Fig. 3.2 Flow chart for $NiFe_2O_4$ powder preparation

3.4 Preparation of bismuth ferrite and nickel ferrite composite powder

Composite of $0.7BiFeO_3 - 0.3NiFe_2O_4$ has been prepared by mixing the powders using ball milling technique. The so obtained composite powder was pressed in a die using hand hydraulic press with a pressure of 10 ton/cm^2 into pellet form. 5 % Polyvinyl alcohol were added to powder as binding agent prior to pressing. The pressed pellet was sintered at 850^{o}C in tubular furnace in air atmosphere for one hour. The heating and cooling rate was fixed i.e. 5^{o}C/minute. The dielectric measurements were carried out by LCR meter Agilent 4284A (frequency range 20 Hz to 1MHz). For dielectric measurements, the sintered pellets were coated on both sides by Ag paste. *P-E* loop of the pellet were carried out by the scan Agilent 4284A (frequency range 20 Hz to 1MHz).

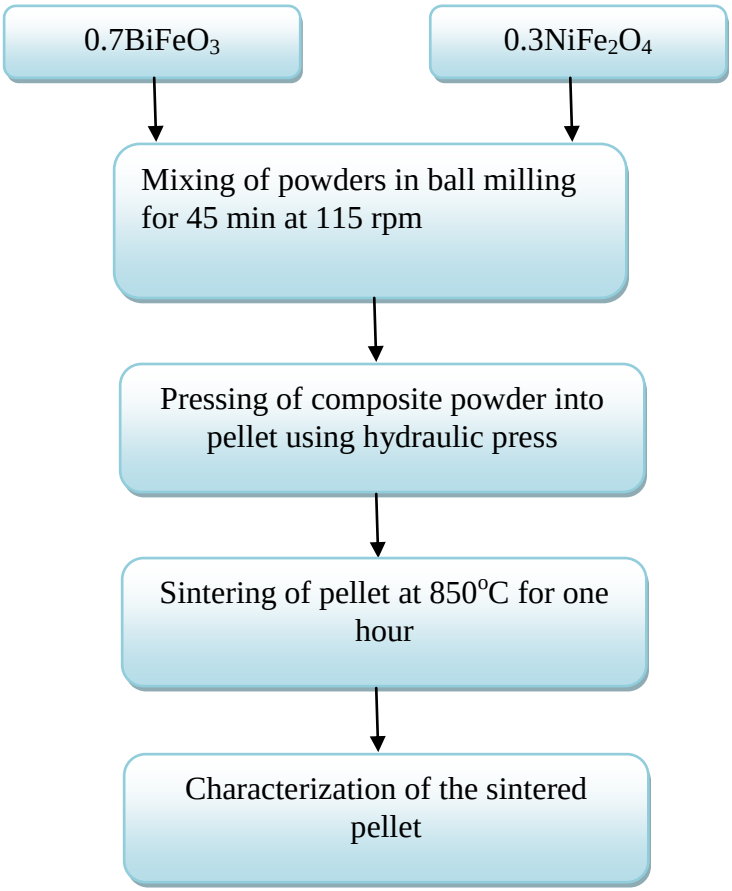

Fig. 3.3 Flow chart for composite

CHAPTER-4
RESULTS AND DISCUSSION

4.1 Phase Characterization

Fig. 4.1 shows the room temperature XRD pattern of $BiFeO_3$ powder prepared by sol gel method and annealed at 800°C. The peaks were matched with JCPDS card no. 861518. It was found that the majority of powder shows rhombohedrally distorted perovskite $BiFeO_3$ phase. Besides the formation of BFO R-phase, the small impurity phases, such as $Bi_2Fe_4O_9$ was also observed. The crystallite size was calculated using Debye-Scherrer equation given below:

Crystallite size (Å) = $0.9\lambda/\beta \cos\theta$

where, λ is wavelength of X-rays

β is full width at half maxima (FWHM)

θ is the angle in degrees

The calculated average crystallite size was 32.88 nm.

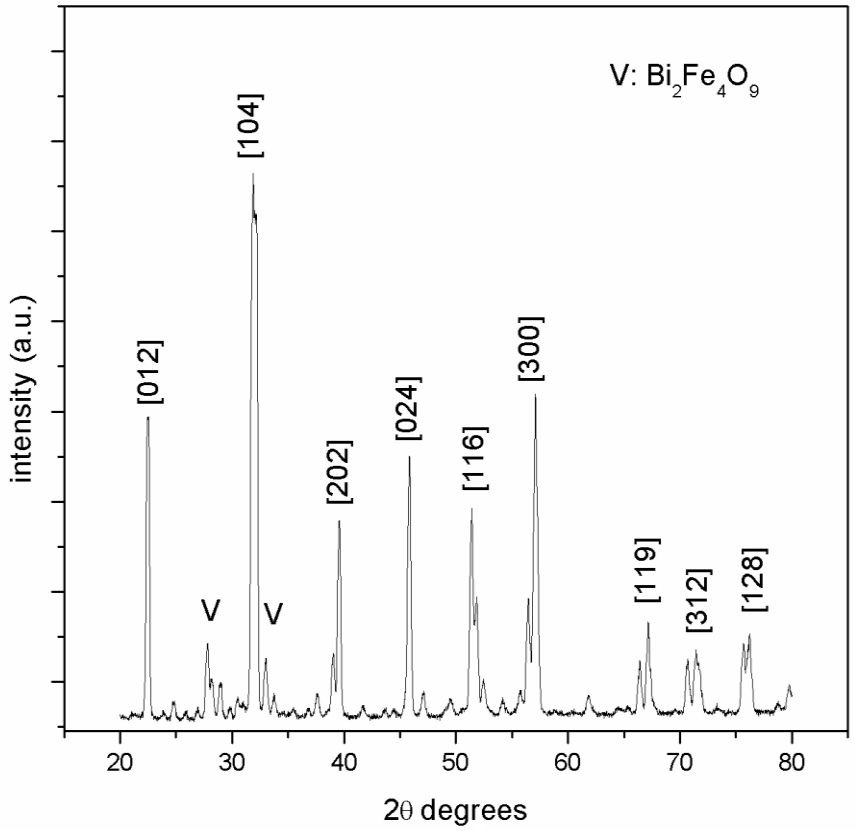

Fig. 4.1 XRD pattern of BFO powder annealed at 800°C

Fig. 4.2 shows the room temperature XRD pattern of $NiFe_2O_4$ powder prepared by sol-gel method and annealed at 1100^oC. The peaks were matched with JCPDS card no.741913. Single phase $NiFe_2O_4$ were obtained. No evidence of impurity phases was observed. The sol-gel derived nickel ferrite has cubic structure with Fd3m phase. The crystallite size was calculated from Scherrer formula and is found to be 120.33 nm.

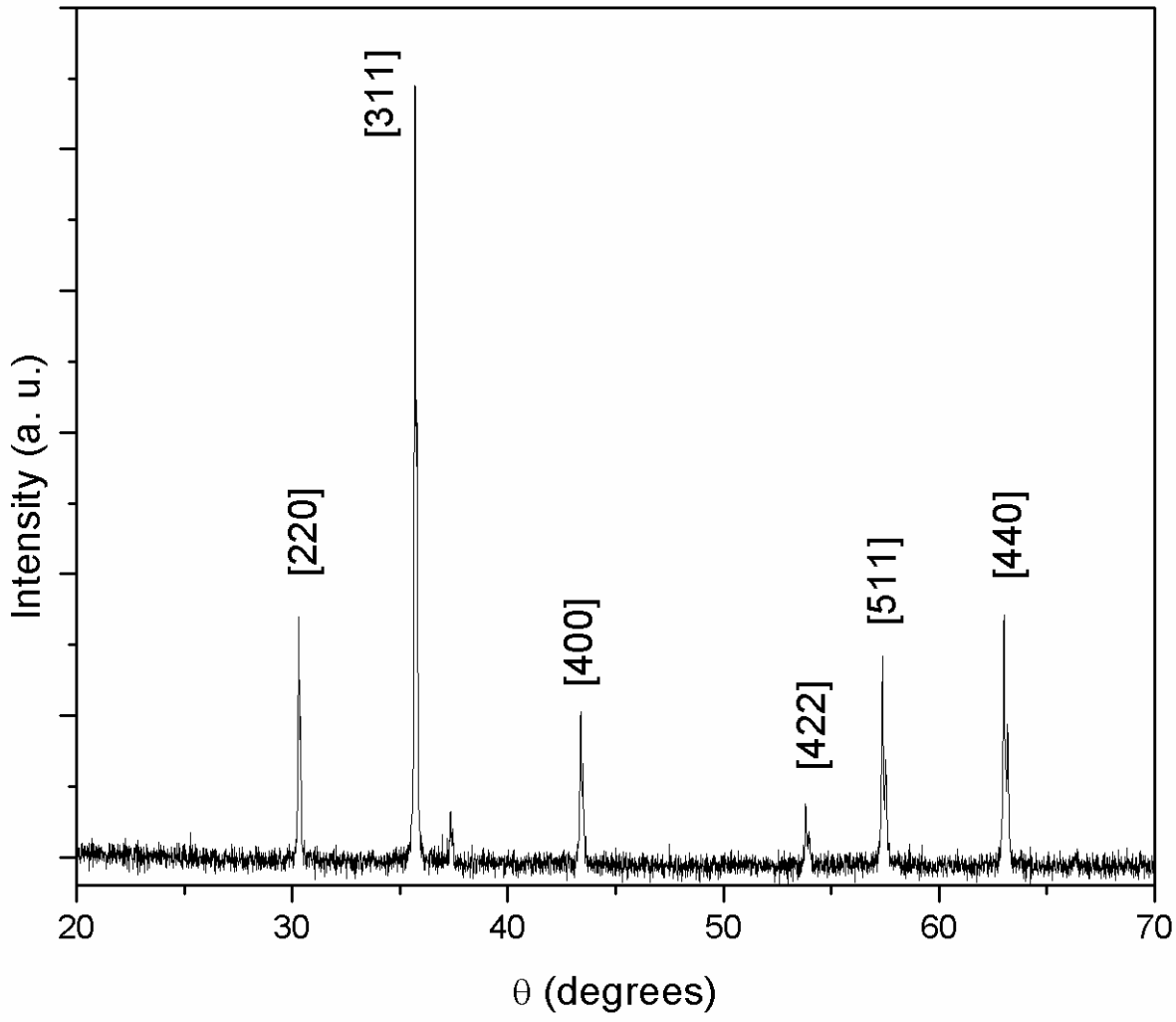

Fig. 4.2 XRD pattern of $NiFe_2O_4$ powder annealed at 1100^oC

4.2 Dielectric properties

Fig. 4.3 shows the room temperature dielectric constant measurements with respect to frequency in the region of 20 Hz to 1 MHz of $BiFeO_3$ and $0.7BiFeO_3$ -0.3 $NiFe_2O_4$ pellets sintered at 850^oC for one hour using LCR meter. It was found that dielectric constant was higher in the lower frequency region. It decreases with further increase in frequency and becomes almost constant at higher frequency region. Such behaviour is seen because at low

frequencies all types of polarization contribute. As the frequency is further increased only electronic and ionic polarisation contributes which is the reason for the decrease in the dielectric constant. With addition of nickel ferrite the dielectric constant of $BiFeO_3$ decreases which may be accepted on the basis of Ginzburg-Landau theory which explained the origin of anomaly in dielectric constant on the magnetic order of ferroelectromagnets [54].

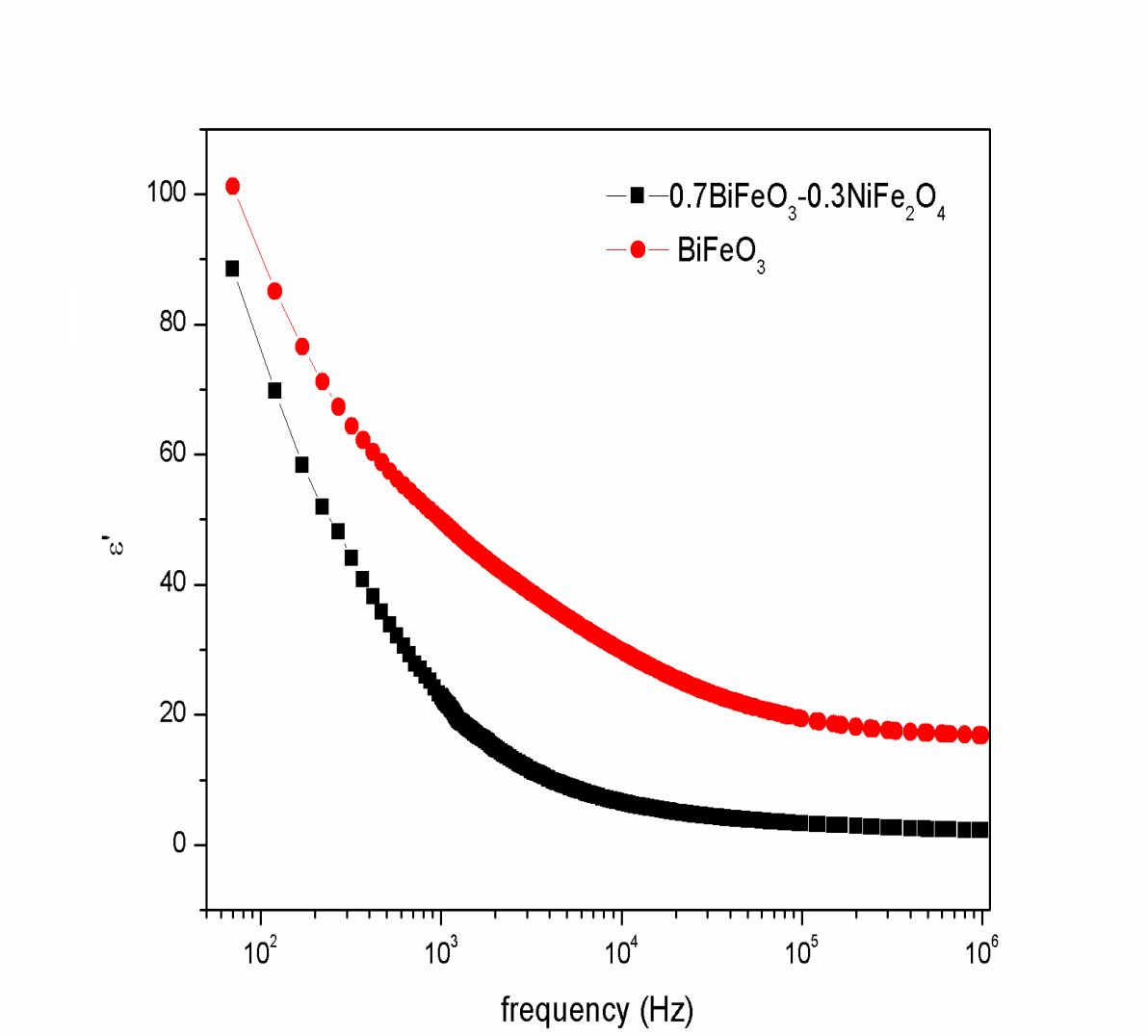

Fig 4.3 *RT* variation of dielectric constant with frequency.

Table 1 Dielectric parameters of (1-x) $BiFeO_3$- x$NiFe_2O_4$ (x=0, 0.3):

Sample name/ Frequency	$BiFeO_3$	0.7$BiFeO_3$ -0.3$NiFe_2O_4$
10^2	85.77	80.96
10^3	49.67	21.98
10^4	29.51	6.02
10^5	19.03	3.07
10^6	16.93	1.4

Fig 4.4 shows the room temperature dielectric loss measurements with respect to frequency in the region of 20 Hz to 1 MHz of $BiFeO_3$ pellet and 0.7$BiFeO_3$ -0.3 $NiFe_2O_4$ sintered at 850^oC for one hour using LCR meter. It was observed that dielectric losses in case of pure $BiFeO_3$ are less than that of 0.7$BiFeO_3$-0.3$NiFe_2O_4$ composite, which supports the large dielectric constant of pure bismuth ferrite.

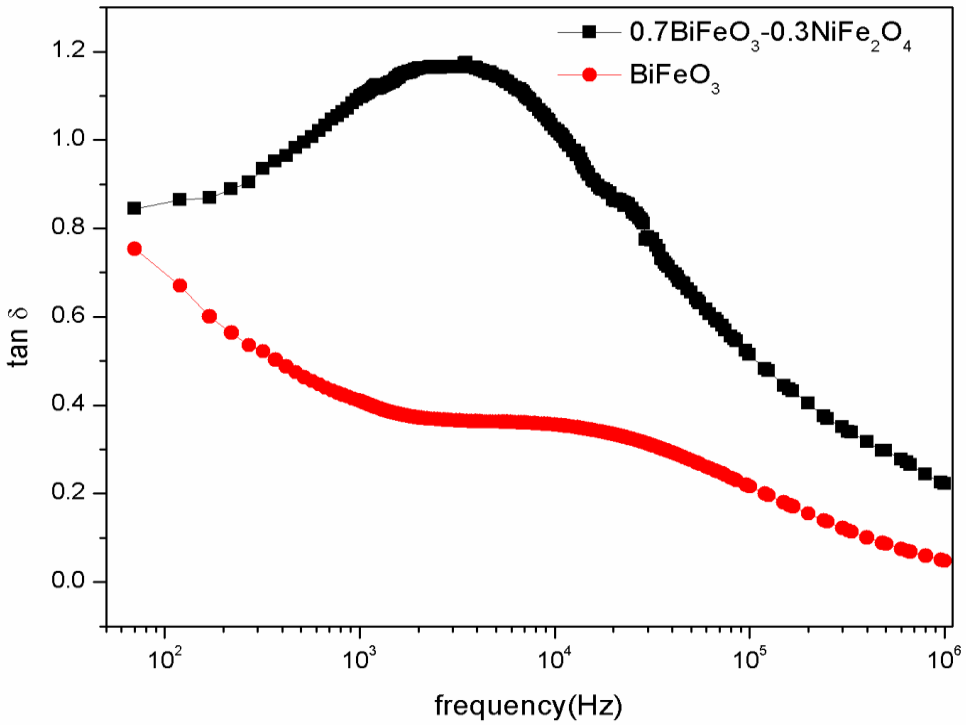

Fig. 4.4 *RT* variation of dielectric loss with frequency.

4.3 *P-E* loop measurement

To study ferroelectric properties, *P-E* hysteresis loop were recorded for both the samples.

Fig. 4.5 shows *P-E* hysteresis loop of pure $BiFeO_3$ confirming the ferroelectric nature of $BiFeO_3$. The value of coercive field, remnant polarization and saturation polarization are given in table 2.

Fig. 4.6 shows the ferroelectric nature of $BiFeO_3$ - $NiFe_2O_4$ composite. A dilution effect was observed from the figure 4.6 i.e. with addition of nickel ferrite in $BiFeO_3$, there is decrease in ferroelectricity of $BiFeO_3$ due to magnetic nature of nickel ferrite. From figure it is also observed that there is asymmetry between positive coercive field and negative coercive field value. This shift in the coercive field value could be attributed to the some internal stress due to different electrode interfaces. Probably different work functions and different densities of interface states might be acting as traps [55].

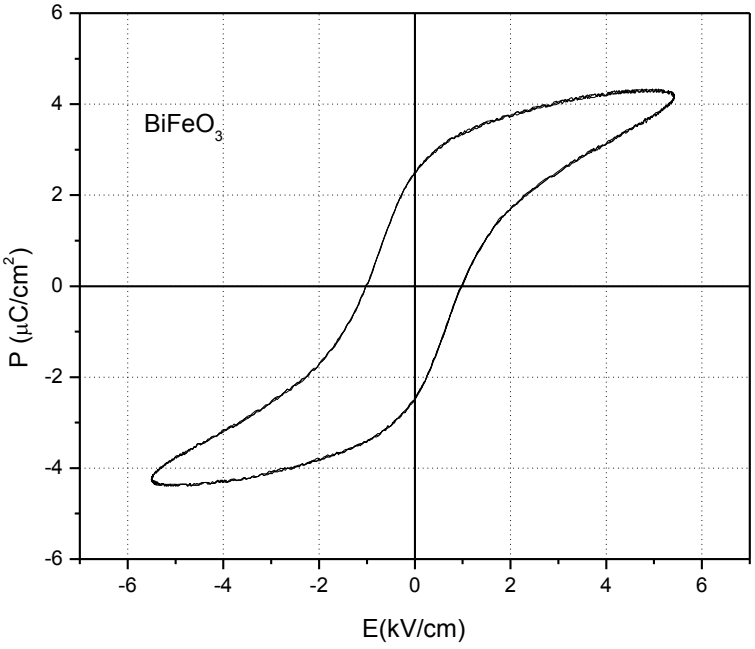

Fig. 4.5 *P-E* loop of $BiFeO_3$

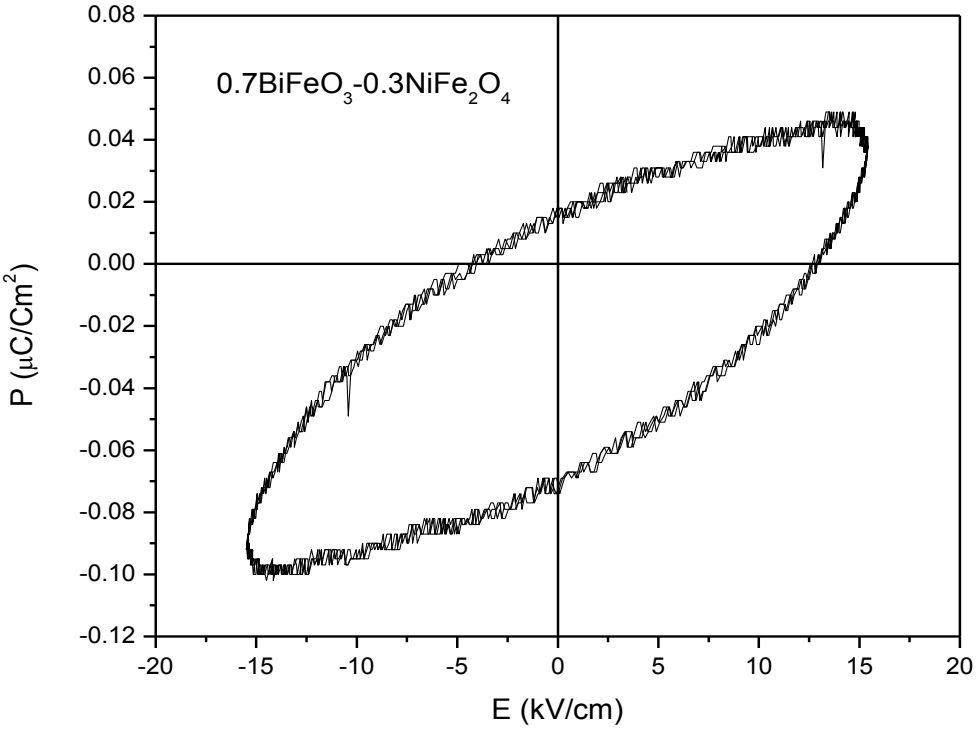

Fig. 4.6 *P-E* loop of $0.7BiFeO_3$-$0.3NiFe_2O_4$

Table 2 Ferroelectric parameters of (1-x) $BiFeO_3$- $xNiFe_2O_4$ (x=0, 0.3):

Sample name	P_s (μC/cm^2)	P_r (μC/cm^2)	E_c (kV/cm)
$BiFeO_3$	22.47	5.46	2.484
$0.7BiFeO_3$-$0.3NiFe_2O_4$	0.32	0.07	16.96

The larger value of the coercive field for bismuth ferrite-nickel ferrite composite may be attributed due to the fact that nickel ferrite shows the pinning effect to depolarization, and hence the larger value of the coercive field for the system in which nickel ferrite is embedded in bismuth ferrite.

Conclusion

Bismuth ferrite powder and nickel ferrite powder were successfully made by sol-gel method and characterized by X-ray diffraction (XRD). Besides the formation of single phase $BiFeO_3$ an impurity phase was also observed. However, single phase $NiFe_2O_4$ were obtained. Composite structure of bismuth ferrite and nickel ferrite ($0.7BiFeO_3$-$0.3NiFe_2O_4$) was made and their dielectric and ferroelectric properties were compared with pure $BiFeO_3$. The dielectric properties studies showed that $0.7BiFeO_3$-$0.3NiFe_2O_4$ has smaller dielectric constant value and shows more dielectric losses as compared to pure $BiFeO_3$. The dielectric constant value at room temperature for the composite was found to be 6.02 as compared to 29.51 for pure bismuth ferrite at 10^2 Hz. The ferroelectric studies at room temperature showed a hysteresis loop for pure bismuth ferrite with remnant polarization of $5.46\mu C/cm^2$ at coercive field of 2.48kV/cm for $BiFeO_3$ as compared to asymmetrical oval shaped hysteresis loop for $0.7BiFeO_3$-$0.3NiFe_2O_4$ composite with remnant polarisation of $0.07\mu C/cm^2$ at coercive field of 16.96kV/cm.

Future Scope

$BiFeO_3$-$NiFe_2O_4$ composites can be studied for narrow compositional range and their magnetic and magnetoelectric coupling can be investigated.

REFERENCES

1. J. C. Maxwell, *Phil. Trans. R. Soc. Lond.* **155,** 459–512 (1865).
2. L.D.Landau, & E. M. Lifshitz, *The Classical Theory of Fields* 2nd edn (Pergamon, London, 1962).
3. P.Curie, *J. Physique* **3**, 393 (1894).
4. L. D. Landau and E. M. Lifshitz, *Electrodynamics of continuous media*. (Fizmatgiz, Moscow), (1959).
5. W. Eerenstein, N. D. Mathur and J. F. Scott, *Nature* **442**, 759 (2006).
6. H.Béa, M.Gajek, M.Bibes and A.Barthélémy, *J. Phys.:Condens. Matter*. **20**, 434221 (2008).
7. N.A. Hill, *J. Phys. Chem. B* **104**, 6694 (2000).
8. H. Schmid, *Ferroelectrics* **161**, 1–28 (1994).
9. D. Khomskii, *Physics* **2**, 20 (2009).
10. J. B. Goodenough and J. M. Longo, Landolt-Börnstein, *Numerical data and Functional Relations in Science and Technology*, New Series Vol. **III.** 4 (Springer, Berlin, 1970).
11. T. Mitsui, Landolt-Börnstein, *Numerical data and Functional Relations in Science and Technology*, New Series Vol. **16** (1) (Springer, Berlin, 1981).
12. S.W.Cheong , Maxim Mostovoy, *Nature Materials* **6,** 13 (2007).
13. Special issue, *J. Phys. Condens. Matter* **20**, 434201–434220 (2008).
14. B. B.van Aken et al., *Nature Mater.* **3**, 164 (2004).
15. T. Kimura, *Nature* **426,** 55 (2003).
16. N. Hur et al., *Nature* **429,** 392 (2004).
17. T. Arima, *J. Phys. Soc. Jpn***. 76**, 073702 (2007).
18. Y. J. Choi et al., *Phys. Rev. Lett*. **100,** 047601 (2008).
19. J.F.Scott, *Nature Mater.* **6,** 256 (2007).
20. M. Gajek, M. Bibes, S. Fusil, K. Bouzehouane, J. Fontcuberta, A. Barthélémy and A. Fert, *Nature Mater.* **6,** 296 (2007).
21. M. Vopsaroiu, J. Blackburn, A. Muniz-Piniella, and M. G. Cain, *J. Appl. Phys.* **103**, 07F506 (2008).
22. G.Catalan and J.F.Scott, *Adv. Mater.* **21,** 2463 (2009).
23. A. Moreira dos Santos, S. Parashar, A. R. Raju, Y. S. Zhao, A. K. Cheetham and C. N. R. Rao, *Solid State Commun*. **122,** 49 (2002).

24. S. Niitaka, M. Azuma, M. Takano, E. Nishibori, M. Takata, M. Sakata, *Solid State Ionics* **172,** 557 (2004).
25. N. A. Hill and K. M. Rabe, *Phys. Rev*. B **59,** 8759 (1999).
26. V. A. M. Brabers, Handbook of Magnetic Materials, vol.**8** (1995).
27. M. P´enicaud, B. Siberchicot, C. B. Sommers, J. K¨ubler, JMMM **103** 212 (1992).
28. Pannaparayil T, Marande R, Komarneni S,, Sankar SG, J. Appl. Phys. **64**, 5641 (1988).
29. Goldmann A (1988) In: Levenson (ed) Electronic Ceremics. Marcel Dekker, New York, p **170** (1988).
30. Dormann JL, Fiorani D (1992) Magnetic properties of Fine Particles, North Holland, Amsterdam.
31. U. Müller, Inorganic structural chemistry, Wiley-VCH, (1999**).**
32. D. Shriver, P. Atkins, Inorganic chemistry, Wiley-VCH, second edition, (1997).
33. Binu P Jacob, Ashok Kumar, R P Pant, Sukhvir Singh And E M Mohammed, Bull. Mater. Sci., Vol. **34**, No. 7, pp. 1345–1350 (2011).
34. A.S. Albuquerque, J.D. Ardisson, W.A.A. Macedo, J.L. LoH pez, R. Paniago, A.I.C. Persiano, Journal of Magnetism and Magnetic Materials 226, **230** (2001).
35. T. Abraham, Am. Ceram. Soc. Bull **73**, 62 (1994).
36. E. Olsen, J. Thonstad, J. Appl. Electrochem. **29**, 293 (1999).
37. S.E. Ziemniak and M. Hanson, Corrosion behaviour of NiCrFe alloy 600 in high temperature, hydrogenated water, Corrros. Sci. **47** (2005).
38. Jong Kuk Kim , Sang Su Kim , Won-Jeong Kim, Materials Letters **59**, 4006 – 4009 (2005).
39. F. Chen, Q. F. Zhang, J. H. Li, Y. J. Qi, C. J. Lu et al., Appl. Phys. Lett. **89**, 092910 (2006).
40. Ratnakar Pandu, K L Yadav, Amit Kumar, P Ravinder Reddy, A V S S K S Gupta, Indian J. of Engineering and Materials Sciences Vol.**17**, pp.481-485 (2010).
41. . Tadej Rojac,Marija Kosec, Bojan Budic, Nava Setter, and Dragan Damjanovic (J. Appl. Phys. **108**, 074107 (2010).
42. . Zhiwu Chen, Guanghui Zhan, Xinhua He, Hu Yang, and Hao Wu, Cryst. Res. Technol. **46**, No. 3, 309 – 314 (2011).
43. . Chandrashekhar P. Bhole, Archives of Appl. Science Research, **3** (5):384-389 (2011).

44. A.S. Albuquerque, J.D. Ardisson, W.A.A. Macedo, J.L. LoH pez, R. Paniago, A.I.C. Persiano, J. of Magnetism and Magnetic Materials **226**, 230, 1379, 1381 (2001).
45. J. Azadmanjiri and S. A. Seyyed Ebrahimi, The Physics of Metals and Metallography Vol. **102**, Suppl. 1, pp. S21–S23 (2006).
46. Binu P Jacob, Ashok Kumar, R P Pant, Sukhvir Singh and E M Mohammed**,** Bull. Mater. Sci., Vol. **34**, No. 7, pp. 1345–1350.(2011**).**
47. P. Sivakumar, R. Ramesh, A. Ramanand,S. Ponnusamy, C. Muthamizhchelvan, Materials Research Bulletin Volume **46**, Issue 12, Pages 2204–2207 (2011).
48. Haimei Zheng, Oian Zhan, Florin Zavaliche, Matt Sherbwne, Florian Straub, Maria P. Cruz, Long Oing Chen, Uli Dahmen and R. Ramesh, Nano Lett. **6** (2006).
49. Q. Zahan, R. Yu, S.P. Crane, H. Zheng, C. Kisielowski, R. Ramesh, *Appl. Phys. Lett*. **89,** 172902 (2006).
50. S. P. Crane, C. Bihler, M. S. Prant, S. T. B. Goennenwein, M. Gajek, R. Ramesh, *J.Magn. and Mag. Mat*. **321** (2009).
51. Li Yan, Zengping Xing, Zhiguang Wang, Tao Wang, Guangyin Lei, Jiefang Li, D. Viehland *Appl. Phys. Lett*. **94,** 192902 (2009).
52. S. Narendra Babu, Jen-Hwa Hsu, Y. S. Chen, and J. G. Lin, *J.App. Phys*. 107(2010).
53. Poonam Uniyal, K. L. Yadav, *J. Alloys and Compds*. **492** (2010).
54. Amit Kapoor, K. L. Yadav, Hemant Singh, Ratnakar Pandu, P. Ravinder Reddy, *Physica* B **405** (2010).
55. Renu Rani, Parveen Kumar, Sangeeta Singh, J. K. Juneja, K. K. Raina & Chandra Prakash Ferroelectrics Letters Section, **38**:4-6, 108-113 (2011).